Anomalous Coulomb Drag between InAs Nanowire and Graphene Heterostructures

Richa Mitra, Manas Ranjan Sahu, Kenji Watanabe, Takashi Taniguchi, Hadas Shtrikman,
A. K. Sood, and Anindya Das

Anomalous Coulomb Drag between InAs Nanowire and Graphene Heterostructures

Richa Mitra[1], Manas Ranjan Sahu[1], Kenji Watanabe[2], Takashi Taniguchi[2], Hadas Shtrikman[3], A.K Sood[1] and Anindya Das[1]

[1]*Department of Physics,Indian Institute of Science, Bangalore, 560012, India.*
[2]*National Institute for Materials Science, Namiki 1-1, Ibaraki 305-0044, Japan.*
[3]*Department of Physics, Weizmann Institute of Technology, Israel.*
(Dated: February 24, 2020)

Correlated charge inhomogeneity breaks the electron-hole symmetry in two-dimensional (2D) bilayer heterostructures which is responsible for non-zero drag appearing at the charge neutrality point. Here we report Coulomb drag in novel drag systems consisting of a two-dimensional graphene and a one dimensional (1D) InAs nanowire (NW) heterostructure exhibiting distinct results from 2D-2D heterostructures. For monolayer graphene (MLG)-NW heterostructures, we observe an unconventional drag resistance peak near the Dirac point due to the correlated inter-layer charge puddles. The drag signal decreases monotonically with temperature ($\sim T^{-2}$) and with the carrier density of NW ($\sim n_N^{-4}$), but increases rapidly with magnetic field ($\sim B^2$). These anomalous responses, together with the mismatched thermal conductivities of graphene and NWs, establish the energy drag as the responsible mechanism of Coulomb drag in MLG-NW devices. In contrast, for bilayer graphene (BLG)-NW devices the drag resistance reverses sign across the Dirac point and the magnitude of the drag signal decreases with the carrier density of the NW ($\sim n_N^{-1.5}$), consistent with the momentum drag but remains almost constant with magnetic field and temperature. This deviation from the expected T^2 arises due to the shift of the drag maximum on graphene carrier density. We also show that the Onsager reciprocity relation is observed for the BLG-NW devices but not for the MLG-NW devices. These Coulomb drag measurements in dimensionally mismatched (2D-1D) systems, hitherto not reported, will pave the future realization of correlated condensate states in novel systems.

Correlated electronic states continue to be the focus of the condensed matter community, thanks to their rich complexity in physics and fascinating technological potential in the near future. Over the years the search for realizing highly correlated states have led to the discovery of novel many-body states like excitonic condensate states [1–4], fractional quantum Hall states [5, 6], Luttinger liquid phase[7–10] etc. Coulomb drag has proven to be the quintessential tool for probing the electron-electron interaction in correlated systems and studied in diverse set of systems like 2D electron gas (2DEG) based (AlGaAs/GaAs) heterostructures [1, 2, 4, 11–14] to quantum wires [7–10] . In Coulomb drag, current (I_D) passing in one of the layers produces an open circuit voltage (V_D) in the other layer without any particle exchange. Very recently, graphene based heterostructures [15–19] have revealed intriguing feature of the drag signal at the Dirac point [15, 17, 18]; namely that it can have both positive [15] and negative [18] amplitudes. A puzzling feature is its temperature dependence which shows monotonic behavior with a maximum at the lowest temperature in BLG [18] whereas non-monotonic variation with a maximum at an intermediate temperature (~ 100K) for MLG [15]. The drag signal at the Dirac point can not be explained by the conventional momentum drag mechanism involving the momentum transfers from the drive to the drag layer, and hence two new mechanisms; namely Energy drag [20–22] and inhomogeneous momentum drag [23] have been proposed.

A new drag system consisting of 2D graphene and a confined 1D nanowire or nanotube, not only has a potential for probing the graphene locally, but also the dimensionally mismatched Coulomb drag system can potentially become the foreground for studying the effect of dimension on scattering mechanisms in Coulomb drag [25, 26]. This kind of drag system is expected to show novel quantum phases in the strong coupling regime [27] in addition to being a tool for studying the graphene hydrodynamics near the Dirac point [28]. With this motivation we have carried out the Coulomb drag experiments in MLG-InAs NW and BLG-InAs NW devices as a function of density (n), temperature (T) and magnetic field (B). The MLG-NW devices show a drag resistance ($R_D = V_D/I_D$) maximum around the Dirac point and its dependence on n, T and B establish the Energy drag as the dominant mechanism. In comparison, absence of the drag signal at the Dirac point for the BLG-NW devices and flipping sign across the Dirac point with negligible dependence on T and B suggest the dominance of momentum drag mechanism.

The device and measurement configuration are schematically presented in Fig. 1a. All the devices comprise of heterostructures of hexagonal boron nitride (hBN) encapsulated graphene stack and InAs NW with diameter between 50 to 70 nm. The heterostructures were assembled by the standard hot pick up technique [29, 30], where the ~ 10 nm thick top hBN of the graphene stack separates the graphene channel and the NW (SI-1 of Supplemental Material [24]). The inhomogeneity (δn) of graphene is $\sim 2.5 \times 10^{10}/cm^2$, which cor-
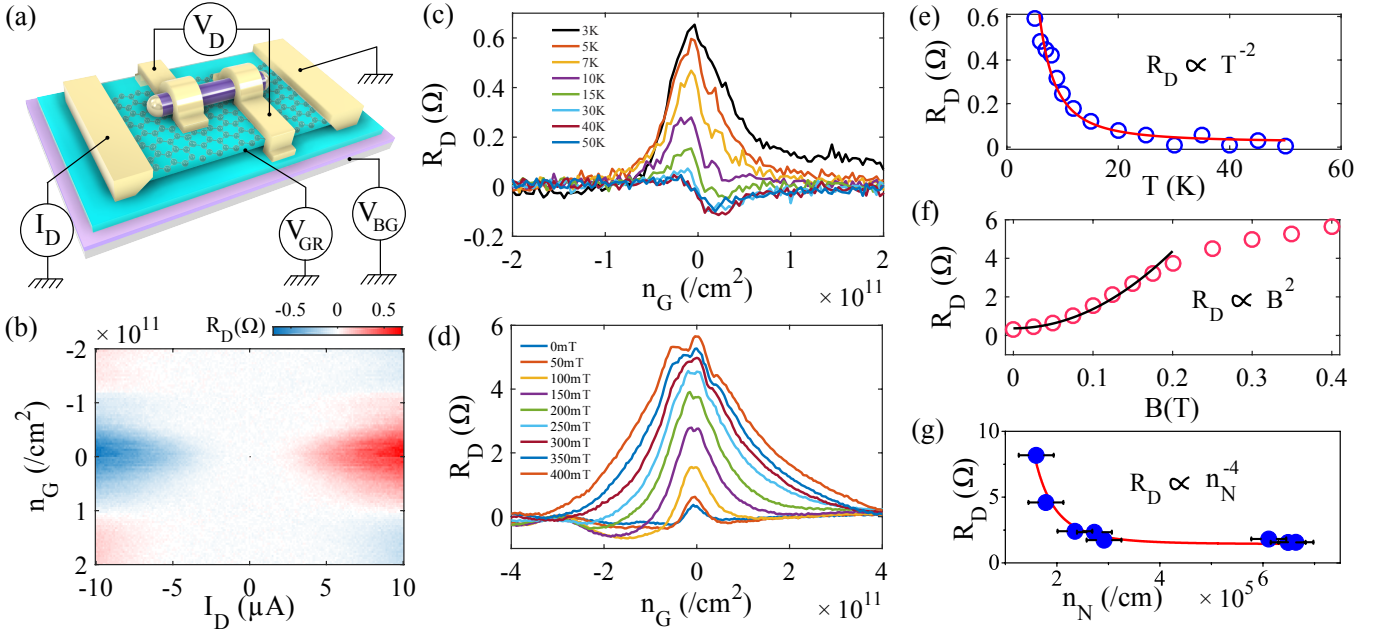
FIG. 1. (a) Device schematic : The heterostructure consists of a InAs nanowire on top of a hBN encapsulated graphene stack assembled on Si/SiO_2 substrate. (b) 2D colormap of R_D at T=1.5K plotted against the I_D and n_G for the D1 device (MLG-NW). (c) Response of the R_D at different temperatures. (d) R_D versus n_G plot for different magnetic fields at T=1.5K. (e) Peak values of the R_D (blue circles) plotted with temperature. R_D decreases with temperature and fits (red solid line) well with $R_D \propto T^{-2}$. (f) The pink open circles are the peak value of R_D plotted with magnetic field at T=1.5K. The black solid line shows data upto 200mT fits well with B^2. (g) R_D at the Dirac point as a function of n_N at T=1.5K. The solid line is an overlay of n_N^{-4} with the data. The errorbars in n_N have been estimated from different sweeps of measurements of device shown in Fig S-3B (a) of the Supplemental Material [24].

responds to a Fermi energy broadening of $\Delta_0 \sim 15 meV$ and $\sim 0.5 meV$ for MLG and BLG, respectively. The NWs could only be electron doped due to Fermi energy pinning near the conduction band. The 1D nature of the NW used is ascertained by measuring the electrical conductance as a function of the V_{BG} for shorter channel length showing participation of 3-5 sub-bands (see SI-1E of Supplemental Material [24]). The charge inhomogeneity in the NW was investigated by measuring the temperature-dependent conductance as shown in Fig. S-1F of Supplemental Material [24], which suggests the localization length of $\sim$ 100-200 nm. All the measurements were done in a He4 cryostat in the temperature range of 1.5K to 200K.

The drag measurements were performed by the DC technique, where I_D was passed through the graphene and V_D was measured on the NW as shown in Fig. 1a or vice versa. The carrier density of the graphene (n_G) and NWs (n_N) were tuned by the SiO_2 back gate (V_{BG}) and by a voltage (V_{GR}) between the graphene and the NW (SI-2 of Supplemental Material [24]). In our DC measurements, the drag signal contains a predominant flipping component (sign reversal of the drag voltage with I_D) together with a small non-flipping component. Here, we present the extracted flipping part (in the linear regime) as mentioned in section SI-2B of Supplemental Material

[24], which is consistent with the drag signal measured by the low-frequency AC (at 7Hz) technique (SI-2 of Supplemental Material [24]). The tunneling resistance of the $\sim$ 10nm thick hBN between the graphene and NWs was more than $5-10 G\Omega$ in all the devices. We have used two MLG-NW (D1, D2) and two BLG-NW (D3, D4) devices for the drag measurements.

Figure 1b shows the 2D colormap for the MLG-NW device (D1) at T=1.5K and $n_N \sim 4 \times 10^5$ cm^{-1}, where R_D is plotted with I_D varying from -10μA to +10μA and n_G varying from 0 to $2 \times 10^{11}/cm^2$ for both electron and hole doping. The drag signal peaks near the Dirac point and subsequently decays at higher n_G. Figure 1c shows R_D at different temperatures. The peak magnitude decreases rapidly with temperature as shown by open circles in Fig. 1e. Figure 1d shows the dependence of R_D on magnetic field upto 400 mT at T=1.5K. Notably, we observe a giant increase (by one order of magnitude) of the drag peak with increasing magnetic field as shown by open circles in Fig. 1f. The dependence of the drag peak on n_N measured by varying V_{GR} (SI-3C of Supplemental Material [24]) is shown in Fig. 1g.

Figure 2a shows the 2D colormap for the BLG-NW device (D3), where R_D is plotted as a function of I_D and n_G at T=1.5K for $n_N \sim 1.3 \times 10^5$ cm^{-1}. In contrast to MLG-NW devices, the drag signal flips sign from positive
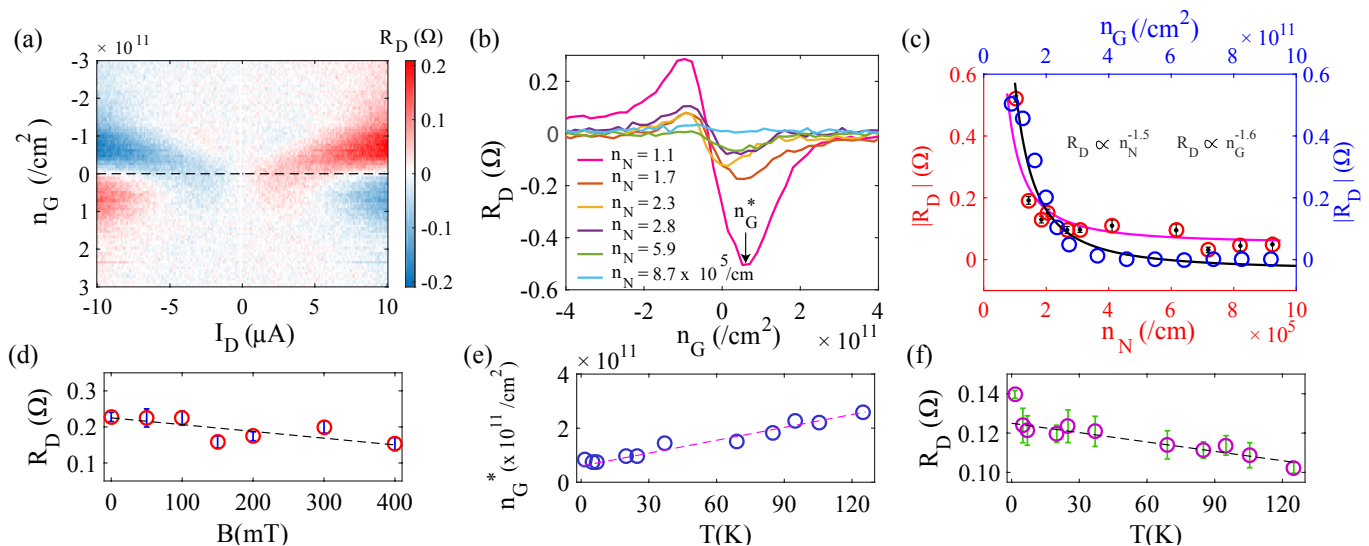
FIG. 2. (a) 2D colormap of R_D with I_D and n_G at $T=1.5$K, $V_{GR} = 1V$ for a BLG-NW device. The horizontal dashed line is the Dirac point of the graphene. (b) R_D versus n_G plot at $T=1.5$K for different n_N tuned by the V_{GR} from 0.9 to 5V. (c) The red circles are the plot for dip value of R_D at different n_N. The variation of the drag signal with n_G at $V_{GR} = 0.9V$ is indicated by the blue open circles. The solid lines are the fitting to $\sim n_N^{-1.5}$ and $n_G^{-1.6}$. (d) The variation of R_D with magnetic field at $T=1.5$K. (e) The position of the dip (n_G^*) of R_D as a function of temperature (raw data in Fig. S-4B of Supplemental Material [24]). (f) The dip value of R_D plotted as a function of temperature. The dashed lines in d, e and f are the guiding lines.

to negative as n_G shifts from holes to electrons across the Dirac point with distinct peak and dip at finite densities of holes and electrons. At the Dirac point the R_D is negligible unlike the MLG-NW device. Figure 2b shows R_D as a function of n_G for different NW densities ($n_N \sim 1$ to 10×10^5 cm^{-1}) tuned by V_{GR}. The blue circles in Fig. 2c quantify how the magnitude of R_D decreases with n_G (for electron side in Fig. 2b) for $n_N = 1.1 \times 10^5$ cm^{-1}, whereas the red circles show the magnitude of the dip of R_D at n_G^* (marked in Fig. 2b) as a function of n_N. Figure 2d shows that R_D at n_G^* for the BLG-NW device remains almost constant with magnetic field (raw data in SI-4A of Supplemental Material [24]), in contrast with the MLG-NW device. Figure 2e and 2f demonstrate the temperature dependence of the drag signal for the BLG-NW device. It can be seen from Supplemental Material [24] Fig. S-4B (raw data) that the peak (hole side) or dip (electron side) position of R_D shifts towards higher carrier density in graphene with increasing temperature for a fixed carrier density of the NW ($n_N \sim 1 \times 10^5$ cm^{-1}). Figure 2e shows the position (n_G^*) and the corresponding value of R_D in Fig. 2f as a function of temperature. Unlike the MLG-NW device, the drag signal in the BLG-NW device clearly displays much less variation with temperature.

The observations of monotonic decrease of drag signal of the MLG-NW device as well as weak dependence of the drag signal of the BLG-NW device on increasing temperature are anomalous as compared to the conventional momentum drag which predicts T^2 [31–34] increase as seen in double-layer MLG heterostructures [15]. Anomaly

in temperature-dependence, specifically, drag signal increasing with lowering temperature has been observed in 2DEG (GaAs-AlGaAs) [11] or 2DEG-graphene [19] heterostructures. The anomalous upturn of the drag signal with lowering temperature at low temperature regime indicated the presence of interlayer excitonic condensation in 2DEG-graphene system [19] or the Luttinger liquid state in quantum wire systems [7]. The possibility of excitonic condensation in our MLG-NW devices is ruled out as the drag peak appears at the Dirac point of graphene with the NW having a finite density.

To explain our results, we first recall the three main mechanisms of the Coulomb drag: (i) homogeneous momentum drag (HMD) - momentum transfers via Coulomb mediated scattering, (ii) inhomogeneous momentum drag (IMD) - momentum transfer in presence of correlated inter-layer charge puddles and (iii) energy drag (ED) - vertical energy transfer in presence of correlated inter-layer charge puddles. Since the HMD signal should be zero at the Dirac point and increases as T^2 in a Fermi liquid [31–34], it can be ruled out as the possible mechanism for our MLG-NW devices. Now, both IMD and Energy drag mechanisms predict a maximum of R_D at the Dirac point due to the presence of correlated inter-layer charge puddles, although the underlying physics is different. The effective momentum theory (EMT) of IMD [23] suggests an increase of the drag signal with temperature in low temperature regime and should decrease when $k_B T > 0.5\Delta_0$. Further, the EMT does not explain the effect of magnetic field on the drag signal. Thus the anomalous decrease with temperature and enhancement

of R_D with magnetic field in our MLG-NW devices is not consistent with the predictions of the IMD.

Coming now to the Energy drag mechanism, a positive correlation of charge inhomogeneities in MLG and NW gives rise to a positive drag peak around the Dirac point due to the combined effect of Coulomb mediated vertical energy transfer and thermoelectric Peltier effect [20]. The Energy drag is expected to increase [22] with magnetic field as B^2 and display a non-monotonic behavior with temperature [20]. Fig. 1f for the MLG-NW device clearly shows B^2 dependence of R_D at lower magnetic field which is consistent with the Energy drag mechanism [20]. To explain the temperature dependence, a quantitative theory of ED in 2D-1D system is required. In the absence of such theory, we appeal to Song et.al for 2D-2D system which shows [20] $R_D \propto \frac{1}{2T\kappa} \frac{\partial Q}{\partial \mu_G} \frac{\partial Q}{\partial \mu_N}$, where $\frac{\partial Q}{\partial \mu}$ is the partial derivatives of the Peltier coefficient Q with respect to the chemical potentials of drive (μ_G) and drag layers (μ_N). The quantity κ is the sum of the thermal conductivities ($\kappa_G + \kappa_N$) of the two layers. For double-layer graphene heterostructures, the Energy drag mechanism [20] generates a non-monotonic temperature behavior where the drag signal increases as T^2 upto a temperature equivalent to $\sim \Delta_0$ and subsequently decreases as T^{-4}. For the MLG-NW devices, the typical value of Δ_0 is $\sim 15meV$ (equivalent to 150K). Hence, according to the Energy drag mechanism, the drag signal should have increased monotonically upto $\sim 150K$. While discussing the Energy drag mechanism, we need to keep in mind that the studies so far assume two identical layers of graphene having similar properties such as mobility, thermal conductivity, electrical conductivity etc. In contrast, we measure the Coulomb drag between two very dissimilar systems: a high mobility 2D graphene sheet and a low-mobility semiconducting 1D NW, with very different electrical transports. More importantly, the NWs have electrical conductivity $\sim 1e^2/h$ and thus poor electronic thermal conductivity (κ_e) as compared to graphene, making phonon contributions to the thermal transport (κ_{ph}) dominant [35]. Hence, $\kappa = \kappa_G + \kappa_N = \kappa_e + \kappa_{ph}$. Since $\kappa_e \propto T$ and κ_{ph} (electron-phonon contribution) $\propto T^5$ ([36, 37]), $\kappa = (aT + bT^5)$, where a and b are the relative contributions from the electronic and the phononic parts. The contribution of the interlayer dielectric hBN to κ_{ph} is expected to be much smaller than that of the NW and hence is not expected to affect the temperature dependence. Using $\frac{\partial Q}{\partial \mu_G} \propto \frac{T^2}{\Delta_0^2}$ at the Dirac point and $\frac{\partial Q}{\partial \mu_N} \propto \frac{T^2}{\mu_N^2}$ at $\mu_N \neq 0$ (SI-5 of Supplemental Material [24] for details), the temperature dependence of R_D is $R_D \propto \frac{T^3}{\mu_N^2 \Delta_0^2 (aT + bT^5)}$. Noticeably, the R_D still has the non-monotonic dependence on temperature, depending on the relative magnitudes of the parameters a and b. The calculated R_D for different values of a/b is shown in Fig. 3a, where one can see that the crossover happens at temperatures near $\sim 1K$ (below our temperature range)
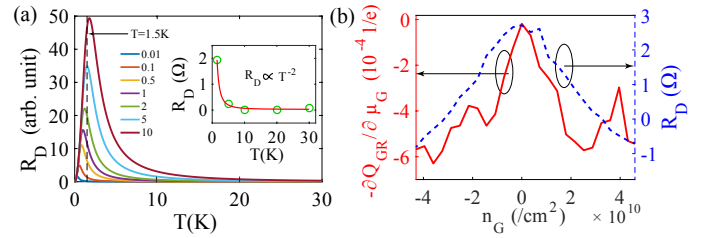

FIG. 3. (a) Theoretically calculated R_D as a function of temperature for several values of a/b ranging from 0.01 to 10. The inset shows the experimental R_D (open circles) as a function of temperature for D2 device with T^{-2} fitting (solid red line). (b) Similarities between $\frac{\partial Q}{\partial \mu}$ (red solid line) and R_D (blue dashed line).

and decreases as T^{-2} consistent with our experimental data (the solid lines in Fig. 1e for D1, and in the inset of Fig. 3a for D2). Furthermore, Fig. 3b shows the similarities between the dependence of R_D and $\partial Q/\partial \mu_G$ on n_G (SI-5 of Supplemental Material [24]), which further strengthens the Energy drag to be the dominant mechanism in MLG-NW devices. Moreover, the effect of carrier density of the NW on the drag peak showing n_N^{-4} dependence (Fig. 1g) is compatible with the Energy drag mechanism as the $\frac{\partial Q}{\partial \mu_N} \propto \frac{T^2}{\mu_N^2} = \frac{T^2}{n_N^4}$ (SI-5 of Supplemental Material [24]) .

We will now discuss the possible drag mechanism for the BLG-NW devices. Drag being almost zero near the Dirac point (Fig. 2a and 2b) rules out Energy drag and IMD, in favour of HMD as a possible mechanism, where $R_D \propto \frac{(k_B T)^2}{n_G^{1.5} n_N^{1.5}}$ is consistent with our result as shown in Fig. 2c (solid lines). However, we do not observe the predicted T^2 increase of the drag signal (Fig. 2f). This can be due to that the drag signal not only slowly varies with increasing temperature but also the shift of the R_D maximum and minimum position (n_G^*) towards higher n_G (Fig. 2e and 2f). This happens due to the temperature-induced Fermi energy broadening, over and above the intrinsic disorder limited Δ_0 (~ 0.5 meV in BLG).

In order to see the effect of dimensionality mismatch on Onsager reciprocity relation, we have measured the drag signal in both NW and graphene as shown in Fig 4. As can be seen the Onsager relation is valid in the BLG-NW device (Fig. 4b), whereas it is violated for the MLG-NW device (Fig. 4a). The violation of Onsager relation has been reported in bilayer 2DEG and 2DEG-graphene devices [2, 14, 19], but the exact reason is not clearly understood. We suggest that the role of different drag mechanisms in Onsager relation can be at play in the dimensionality mismatched devices.

In conclusion, we have performed drag measurements on dimensionally mismatched MLG/BLG-InAs NW heterostructures hitherto not reported. We observe very different drag signals for the MLG-NW and the BLG-NW
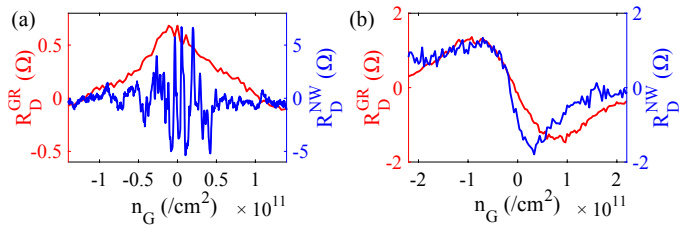
FIG. 4. (a) Onsager in MLG-NW device at T=1.5K. The red line corresponds to the R_D measured on NW whereas the blue line corresponds to the R_D measured on MLG. (b) Similar data for the BLG-NW device.

devices. The MLG-NW devices show a maximum of R_D at the Dirac point and the peak value decreases with increasing temperature as well as with the carrier density of the NW. Further, the drag increases by one order of magnitude with magnetic field. These results show that the Energy drag mechanism is dominant for the Coulomb drag in the MLG-NW heterostructures, where the phononic thermal conductivity of the NWs plays a significant role in reduced drag signal with increasing temperature. In contrast, for the BLG-NW devices, the drag reverses sign across the Dirac point as expected from the momentum drag mechanism, with slow variation with temperature and magnetic field. Our results are promising for realizing the correlated states in dimensionally mismatched novel devices, with different mechanisms at play.

[1] M. Kellogg, I. Spielman, J. Eisenstein, L. Pfeiffer, and K. West, Physical review letters **88**, 126804 (2002).
[2] J. Seamons, C. Morath, J. Reno, and M. Lilly, Physical review letters **102**, 026804 (2009).
[3] J. Li, T. Taniguchi, K. Watanabe, J. Hone, and C. Dean, Nature Physics **13**, 751 (2017).
[4] D. Nandi, A. Finck, J. Eisenstein, L. Pfeiffer, and K. West, Nature **488**, 481 (2012).
[5] J. Eisenstein, G. Boebinger, L. Pfeiffer, K. West, and S. He, Physical review letters **68**, 1383 (1992).
[6] Y. Suen, L. Engel, M. Santos, M. Shayegan, and D. Tsui, Physical review letters **68**, 1379 (1992).
[7] D. Laroche, G. Gervais, M. Lilly, and J. Reno, Science **343**, 631 (2014).
[8] P. Debray, V. Zverev, O. Raichev, R. Klesse, P. Vasilopoulos, and R. Newrock, Journal of Physics: Condensed Matter **13**, 3389 (2001).
[9] M. Yamamoto, M. Stopa, Y. Tokura, Y. Hirayama, and S. Tarucha, Science **313**, 204 (2006).
[10] K. Flensberg, Physical review letters **81**, 184 (1998).
[11] P. Solomon, P. Price, D. Frank, and D. La Tulipe, Physical review letters **63**, 2508 (1989).
[12] T. Gramila, J. Eisenstein, A. H. MacDonald, L. Pfeiffer, and K. West, Physical review letters **66**, 1216 (1991).
[13] M. Kellogg, J. Eisenstein, L. Pfeiffer, and K. West, Physical review letters **90**, 246801 (2003).
[14] A. Croxall, K. D. Gupta, C. Nicoll, M. Thangaraj, H. Beere, I. Farrer, D. Ritchie, and M. Pepper, Physical review letters **101**, 246801 (2008).
[15] R. Gorbachev, A. Geim, M. Katsnelson, K. Novoselov, T. Tudorovskiy, I. Grigorieva, A. H. MacDonald, S. Morozov, K. Watanabe, T. Taniguchi, et al., Nature Physics **8**, 896 (2012).
[16] S. Kim, I. Jo, J. Nah, Z. Yao, S. K. Banerjee, and E. Tutuc, Physical Review B **83**, 161401 (2011).
[17] J. Li, T. Taniguchi, K. Watanabe, J. Hone, A. Levchenko, and C. Dean, Physical review letters **117**, 046802 (2016).
[18] K. Lee, J. Xue, D. C. Dillen, K. Watanabe, T. Taniguchi, and E. Tutuc, Physical review letters **117**, 046803 (2016).
[19] A. Gamucci, D. Spirito, M. Carrega, B. Karmakar, A. Lombardo, M. Bruna, L. Pfeiffer, K. West, A. C. Ferrari, M. Polini, et al., Nature communications **5**, 5824 (2014).
[20] J. C. Song and L. S. Levitov, Physical review letters **109**, 236602 (2012).
[21] J. C. Song, D. A. Abanin, and L. S. Levitov, Nano letters **13**, 3631 (2013).
[22] J. C. Song and L. S. Levitov, Physical review letters **111**, 126601 (2013).
[23] D. Y. Ho, I. Yudhistira, B. Y.-K. Hu, and S. Adam, Communications Physics **1**, 41 (2018).
[24] See Supplemental Material at [URL will be inserted by APS] for addition raw data and detailed discussion on device fabrication, measurement techniques and analysis which includes Refs. [38–51].
[25] Y. M. Sirenko and P. Vasilopoulos, Physical Review B **46**, 1611 (1992).
[26] S. Lyo, Physical Review B **68**, 045310 (2003).
[27] B. Narozhny and A. Levchenko, Reviews of Modern Physics **88**, 025003 (2016).
[28] A. Lucas and K. C. Fong, Journal of Physics: Condensed Matter **30**, 053001 (2018).
[29] L. Wang, I. Meric, P. Huang, Q. Gao, Y. Gao, H. Tran, T. Taniguchi, K. Watanabe, L. Campos, D. Muller, et al., Science **342**, 614 (2013).
[30] F. Pizzocchero, L. Gammelgaard, B. S. Jessen, J. M. Caridad, L. Wang, J. Hone, P. Bøggild, and T. J. Booth, Nature communications **7**, 11894 (2016).
[31] W.-K. Tse, B. Y.-K. Hu, and S. D. Sarma, Physical Review B **76**, 081401 (2007).
[32] B. Narozhny, M. Titov, I. Gornyi, and P. Ostrovsky, Physical Review B **85**, 195421 (2012).
[33] M. Katsnelson, Physical Review B **84**, 041407 (2011).

[34] N. Peres, J. L. Dos Santos, and A. C. Neto, EPL (Europhysics Letters) **95**, 18001 (2011).

[35] Y. Xiong, H. Tang, X. Wang, Y. Zhao, Q. Fu, J. Yang, and D. Xu, Scientific reports **7**, 13252 (2017).

[36] F. Wellstood, C. Urbina, and J. Clarke, Physical Review B **49**, 5942 (1994).

[37] S. K. Srivastav, M. R. Sahu, K. Watanabe, T. Taniguchi, S. Banerjee, and A. Das, Science Advances **5** (2019), 10.1126/sciadv.aaw5798.

[38] K. S. Novoselov, A. K. Geim, S. V. Morozov, D. Jiang, Y. Zhang, S. V. Dubonos, I. V. Grigorieva, and A. A. Firsov, science **306**, 666 (2004).

[39] D. Purdie, N. Pugno, T. Taniguchi, K. Watanabe, A. C. Ferrari, and A. Lombardo, Nature communications **9**, 5387 (2018).

[40] A. Das, Y. Ronen, Y. Most, Y. Oreg, M. Heiblum, and H. Shtrikman, Nature Physics **8**, 887 (2012).

[41] H. Shtrikman, R. Popovitz-Biro, A. V. Kretinin, and P. Kacman, IEEE Journal of Selected Topics in Quantum Electronics **17**, 922 (2010).

[42] D. Suyatin, C. Thelander, M. Björk, I. Maximov, and L. Samuelson, Nanotechnology **18**, 105307 (2007).

[43] C. R. Dean, A. F. Young, I. Meric, C. Lee, L. Wang, S. Sorgenfrei, K. Watanabe, T. Taniguchi, P. Kim, K. L. Shepard, *et al.*, Nature nanotechnology **5**, 722 (2010).

[44] M. R. Sahu, P. Raychaudhuri, and A. Das, Physical Review B **94**, 235451 (2016).

[45] K. Takase, Y. Ashikawa, G. Zhang, K. Tateno, and S. Sasaki, Scientific reports **7**, 930 (2017).

[46] O. Wunnicke, Applied Physics Letters **89**, 083102 (2006).

[47] A. C. Ford, J. C. Ho, Y.-L. Chueh, Y.-C. Tseng, Z. Fan, J. Guo, J. Bokor, and A. Javey, Nano Letters **9**, 360 (2008).

[48] S. Ghatak, A. N. Pal, and A. Ghosh, Acs Nano **5**, 7707 (2011).

[49] A. Ayari, E. Cobas, O. Ogundadegbe, and M. S. Fuhrer, Journal of applied physics **101**, 014507 (2007).

[50] K. Nomura and A. H. MacDonald, Physical review letters **96**, 256602 (2006).

[51] S. D. Sarma, S. Adam, E. Hwang, and E. Rossi, Reviews of modern physics **83**, 407 (2011).